# Memristive Model for Synaptic Circuits

Yang Zhang, Xiaoping Wang, *Member, IEEE*, Yi Li, and Eby G. Friedman, *Fellow, IEEE*

***Abstract*—As a promising alternative for next-generation memory, memristors provide several useful features such as high density, nonvolatility, low power, and good scalability as compared with conventional CMOS-based memories. In this brief, a voltage-controlled threshold memristive model is proposed, which is based on experimental data of memristive devices. Moreover, the model is more suitable for the design of memristor-based synaptic circuits as compared with other memristive models. The effects of memristance variations are considered in the proposed model to evaluate the behavior of memristive synapses within memristor-based neural networks.**

***Index Terms*—Crossbar array, memristor, neural network, synaptic circuits, threshold model.**

## I. INTRODUCTION

As IT has become increasingly difficult to reduce transistor dimensions [1], alternative methods are desired for manufacturing high-density nanoscale memories. One possible candidate is the memristor, which was first theoretically postulated by Chua in 1971 [2], and later, Williams' team presented a memristor at HP in 2008 [3].

As compared with conventional memories based on CMOS technology, memristors provide several advantages such as high density, nonvolatility, low power, and good scalability [4]. Memristors are particularly suitable for realizing neuromorphic systems since these devices are nanoscale two-terminal devices and can be efficiently integrated within crossbar array circuits [5].

Different models of memristive devices have been developed to describe the characteristics of memristors. In 2009, a model for the HP memristor was proposed by Biolek *et al.* [6]. This model does not include a threshold voltage. An approach for modeling a magnetic flux controlled memristor is presented in [7], although this model also lacks a threshold voltage. The TEAM model was proposed in 2013 [8]. This memristor model is however current controlled while most practical memristive devices are voltage controlled. The TEAM model was extended to the "voltage controlled" VTEAM model in 2015 [9]; however, when the inputs are pulse voltages, the derivative of the state variable is constant. An LTSPICE memristive model quantitatively correlated to multiple devices for both sinusoidal and repetitive sweeping inputs is presented in [10]; however, this model does not match changes in the memristance in recent devices [11]–[15]. Existing models do not describe the synaptic behavior of recent memristive devices in memristor-based neural networks. It is therefore of great significance to provide a memristive model that accurately and effectively characterizes artificial synaptic behavior.

In this brief, a new threshold memristor model based on experimental data is proposed, which matches the current–voltage $(I-V)$ characteristics of both sinusoidal and repetitive sweeping inputs and changes in the memristances due to voltage pulses. In addition, the application of the model to a proposed memristor-based synaptic circuit is discussed. The proposed memristor-based synaptic circuit requires fewer amplifiers and resistors as compared with [5]. Moreover, this memristive model can evaluate synapses that consider the effects of variations in the memristance in memristor-based neural networks.

## II. MEMRISTIVE MODEL

An effective memristive model needs to satisfy several requirements. The model should be both sufficiently accurate and computationally efficient. It is desirable for the model to describe the relevant time in closed form. It is also preferable that the model can characterize a memristor composed of different materials. In this section, a model is introduced and compared with different memristive models. The model is also shown to support different types of materials.

As described by Chua in 1971 [2], the charge-controlled memristor is

$$M(q) = \frac{d\phi}{dq} \tag{1}$$

where $M(q)$ is the memristance (in $\Omega$), $\phi$ is the magnetic flux, and $q$ is the electric charge. The HP memristor is described by [13], [16]

$$\left.\begin{array}{l} v(t) = R(t)i(t) \\ R(t) = R_{\mathrm{ON}}\frac{w(t)}{D} + R_{\mathrm{OFF}}\left(1 - \frac{w(t)}{D}\right) \end{array}\right\} \tag{2}$$

$$\frac{dw(t)}{dt} = \mu_v \frac{R_{\mathrm{ON}}}{D} i(t) f\left(w(t)\right) \tag{3}$$

where $w(t)$ is the width of the doped region, $R(t)$ is the memristance, $D$ is the thickness of the $TiO_2$, $\mu_v$ denotes the average ion mobility, $R_{\mathrm{ON}}$ denotes the internal low memristance when the memristor is completely doped, $R_{\mathrm{OFF}}$ denotes the internal high memristance when the memristor is completely undoped, and $i(t)$ and $v(t)$ are, respectively, the current and voltage of

Manuscript received July 28, 2016; accepted August 28, 2016. Date of publication September 1, 2016; date of current version June 23, 2017. This work was supported in part by the State Key Program of the National Natural Science Foundation of China under Grant 61134012; by the National Natural Science Foundation of China under Grant 11271146, Grant 61374150, and Grant 61376130; and by the Doctoral Fund of the Ministry of Education of China under Grant 20130142130012. This brief was recommended by Associate Editor H. H.-C. Iu. *(Corresponding author: Xiaoping Wang.)*

Y. Zhang and X. Wang are with the School of Automation, Huazhong University of Science and Technology, Wuhan 430074, China (e-mail: wangxiaoping@mail.hust.edu.cn).

Y. Li is with the School of Optical and Electronic Information and Wuhan National Laboratory for Optoelectronics (WNLO), Huazhong University of Science and Technology, Wuhan 430074, China.

E. G. Friedman is with the Department of Electrical and Computer Engineering, University of Rochester, Rochester, NY 14627 USA.

Color versions of one or more of the figures in this brief are available online at http://ieeexplore.ieee.org.

Digital Object Identifier 10.1109/TCSII.2016.2605069

1549-7747 © 2016 IEEE. Personal use is permitted, but republication/redistribution requires IEEE permission.
See http://www.ieee.org/publications_standards/publications/rights/index.html for more information.

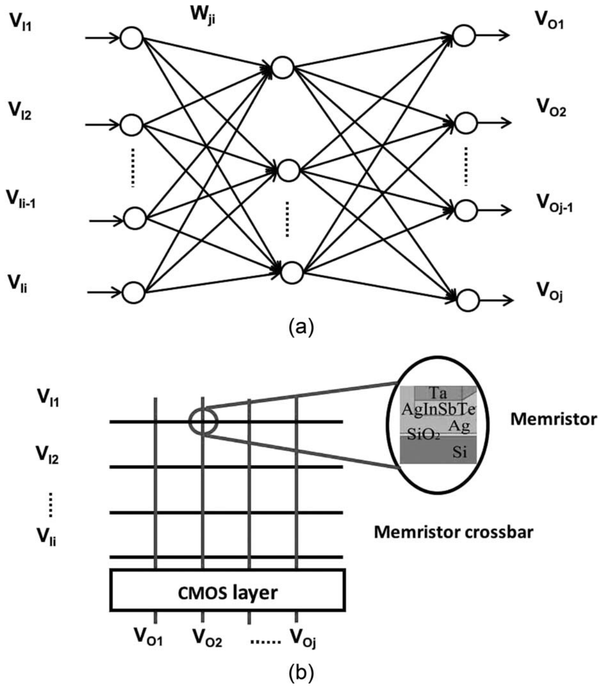


Fig. 1. Architecture of a memristor-based neural network. (a) Artificial neural network. (b) Memristor-based neural network.

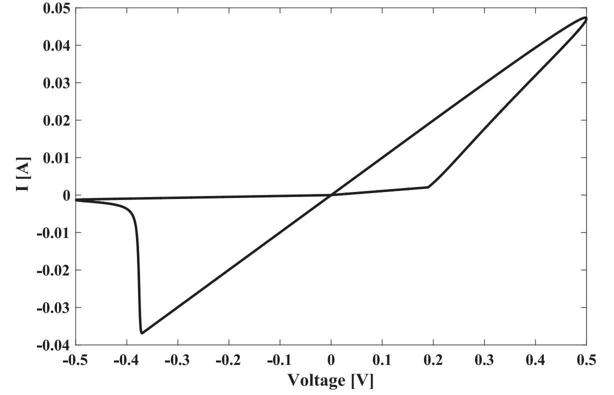


Fig. 2. $I-V$ characteristics of an AIST-based memristor [12].

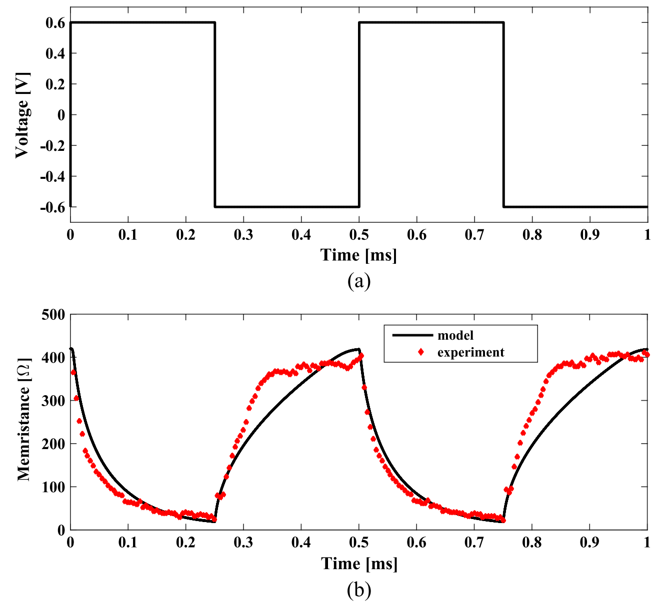


Fig. 3. Change in memristance of an AIST-based memristor [12]. (a) Input voltage, and (b) change in memristance (both simulation and experiment).

the memristor [3]. It is also possible to add a nonlinear ion drift phenomenon, such as a decrease in the ion drift speed close to the bounds, with a window

$$f(w(t)) = 1 - \left(\frac{2w(t)}{D} - 1\right)^{2p} \tag{4}$$

where $p$ is a positive integer.

Memristor-based neural networks are used to imitate biological neural networks, as shown in Fig. 1. To describe the behavior of memristive synapses within memristor-based neural networks, several recent memristive devices have been fabricated based on different materials, such as the AIST-based memristor [11], [12], PCMO-based memristor [13], [14], and $TaO_x$-based memristor [15]. The device behavior of AIST-based, PCMO-based, and $TiO_2$-based memristors, however, cannot be described by the HP model. A new model is therefore proposed here, which matches the behavior of recent memristive devices. The derivative of the state variable in the proposed memristive model is

$$\frac{dw(t)}{dt} = \begin{cases} \mu_v \frac{R_{ON}}{D} \frac{i_{off}}{i(t)-i_0} f(w(t)), & v(t) > V_{T+} > 0 \\ 0, & V_{T-} \leqslant v(t) \leqslant V_{T+} \\ \mu_v \frac{R_{ON}}{D} \frac{i(t)}{i_{on}} f(w(t)), & v(t) < V_{T-} < 0 \end{cases} \tag{5}$$

where $i_0$, $i_{off}$, and $i_{on}$ are constants, $\mu_v$ denotes the average ion mobility, and $V_{T+}$ and $V_{T-}$ are, respectively, positive and negative threshold voltages.

Ag (100 nm)/AgInSbTe (25 nm)/Ta (100 nm) stacked capacitor-like memristors have been fabricated and characterized [12]. Different applied voltages change the memristance of the device. A positive bias is the current flowing from the top Ta electrode through the AgInSbTe memristive layer to the bottom Ag electrode. The $I-V$ characteristics can be evaluated by the proposed model, as shown in Fig. 2. The gradual conductance tuning property under a positive or a negative voltage pulse and the experiment data are also shown in Fig. 3. The proposed model can also be used to evaluate the behavior of a PCMO-based memristor [13], [14] (see Fig. 4) and $TaO_x$-based memristor [15] (see Fig. 5). The relevant parameters of the proposed model used to fit these different memritive devices are listed in Table I.

A comparison of different memristor models is listed in Table II. Since most practical devices are voltage-controlled threshold memristors, three voltage-controlled models (VTEAM [9], Generalized model [10], and the proposed threshold model) are compared. For READ/WRITE circuits, the memristor is treated as a single-bit memory element. For logic circuits, the memristor is considered as a binary-valued element. The threshold characteristics of the memristor are required for logic operations. For a memristor-based neural synapse, the memristance (or conductance) of the memristors gradually changes with bias voltage.

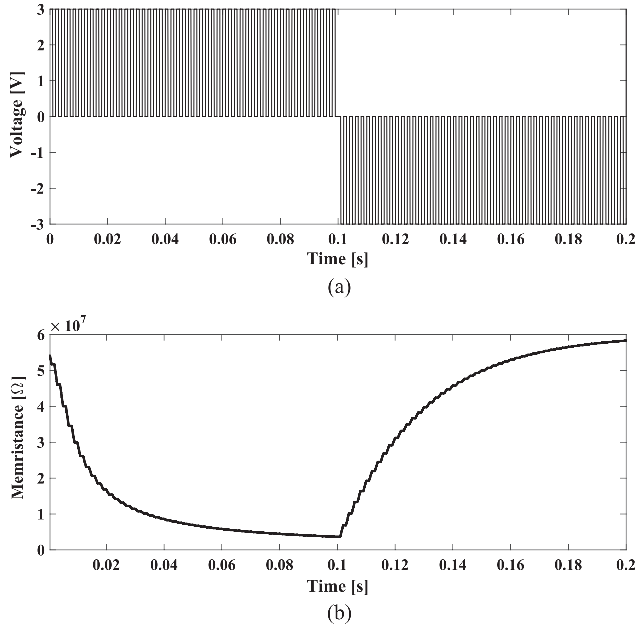


Fig. 4. Change in memristance of a PCMO-based memristor [13], [14]. (a) Input voltage, and (b) change in memristance.

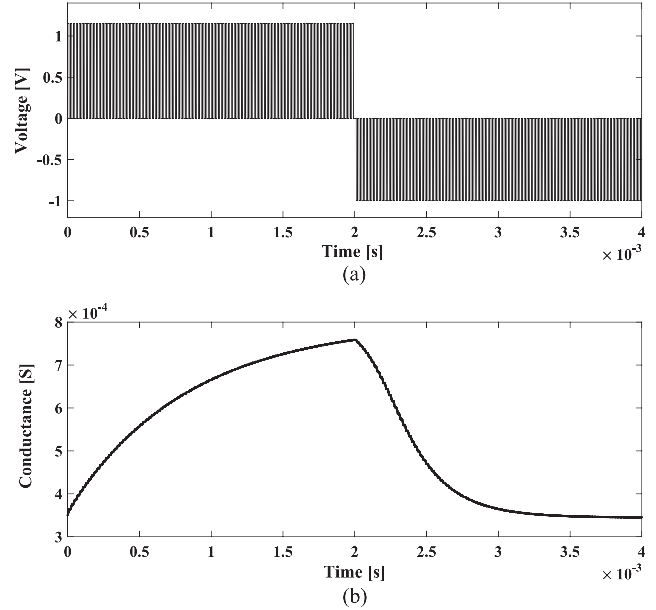


Fig. 5. Change in conductance of a $TaO_x$-based memristor [15]. (a) Input voltage, and (b) change in conductance.

Of the three models, only the proposed threshold model can be used to evaluate synaptic behavior and fit different memristors. For example, to model the behavior of a neural synapse, the conductance of the AIST-based memristor changes during application of 50 potentiation pulses (−0.6 V, 5 $\mu$s) and 50 depression pulses (0.6 V, 5 $\mu$s). The memristance of the PCMO-based memristor changes during application of 50 potentiation pulses (−3 V, 1 ms) and 50 depression pulses (3 V, 1 ms; see Fig. 4) [13], [14], which stores the weight of the neural synapse. In Fig. 5, the conductance of a $TaO_x$-based memristor changes during application of 100 potentiation pulses (−1 V, 10 $\mu$s) and 100 depression pulses (1.15 V, 10 $\mu$s) [15].

The derivative of the state variable in the VTEAM model [9] and the Generalized model [10] is constant when the inputs are pulse voltages. In practical memristive devices, if the inputs are positive pulse voltages, the memristance decreases fast at first and decreases slowly at the end of the transition. If the inputs are negative pulse voltages, the memristance increases fast at first and increases slowly at the end of the transition [shown in Fig. 3(b)]. In the Linear ion drift model [6] and the Magnetic flux controlled model [7], despite no threshold voltage if the inputs are positive pulse voltages, the memristance increases slowly at first and increases fast at the end of the transition, which is opposite the behavior of practical devices.

## III. Application in Synaptic Circuits

In this section, the proposed model is applied to synaptic circuits in Section III-A. Memristors store the synaptic weight in artificial neural networks. The weight change method is presented in Section III-B.

### A. Synaptic Circuits

Assume a neural network system that receives a pair of vectors of size $M$ and $N$: inputs $\mathbf{V}_I \in \mathbb{R}^M$ and outputs $\mathbf{V}_O \in \mathbb{R}^N$. For example, assume $\mathbf{W}$ is an adjustable $N \times M$ matrix and consider the estimator,

TABLE I
Fitting Characteristics of the Proposed Model to Practical Memristive Devices

| *Parameters of Physical Device* | *AIST-based memristor* | *PCMO-based memristor [14]* | *$TaO_x$-based memristor [15]* |
|---|---|---|---|
| $R_{\rm ON}(\Omega)$ | 10 | 1e6 | 1250 |
| $R_{\rm OFF}(\Omega)$ | 420 | 6e7 | 2900 |
| $V_{\rm T-}$ (V) | -0.19 | -2.4 | -0.3 |
| $V_{\rm T+}$ (V) | 0.37 | 1.2 | 0.5 |
| $D$ (nm) | 3 | 3 | 3 |
| $\mu_v$ (m$^2$s$^{-1}\Omega^{-1}$) | 1.6e-12 | 3.2e-15 | 3.8e-14 |
| $i_{\rm on}$ (A) | 1 | 1 | 1 |
| $i_{\rm off}$ (A) | 1e-5 | 1.4e-14 | 5.8e-8 |
| $i_0$ (A) | 1e-3 | 3e-8 | 4e-4 |

$$\mathbf{V}_O = \mathbf{W}\mathbf{V}_I \tag{6}$$

or

$$V_{Oj} = \sum_{i=1}^{M} W_{ji} V_{Ii} \tag{7}$$

where $i = 1, 2, \ldots, M$ and $j = 1, 2, \ldots, N$.

A synaptic array circuit composed of a positive crossbar array of $M^+(G_{ji})$ and a negative crossbar array of $M^-(G'_{ji})$ is shown in Fig. 6. Here, $G_{ji}$ ($G_{ji} = 1/R_{ji}$) and $G'_{ji}$ ($G'_{ji} = 1/R'_{ji}$) are, respectively, the memristor conductance at the crossing point between the $i$th row and the $j$th column in the positive and negative arrays. $V_{Ii}$ is the input voltage applied to the $i$th row. According to Kirchhoff's voltage law, $V_{Oj}$ is

$$V_{Oj} = -\sum_{i=1}^{M}\left(-\frac{R_0}{R_{ji}} \times V_{Ii} \times \frac{R_0}{R_0} + \frac{R_0}{R'_{ji}} \times V_{Ii}\right)$$
$$= \sum_{i=1}^{M} R_0 \times \left(G_{ji} - G'_{ji}\right) \times V_{Ii}. \tag{8}$$

TABLE II
COMPARISON OF DIFFERENT MEMRISTOR MODELS

| *Model* | *Linear ion drift model [6]* | *Magnetic flux-controlled model [7]* | *TEAM [8]* | *VTEAM [9]* | *Generalized model [10]* | *Proposed model* |
|---|---|---|---|---|---|---|
| State variable | $0 \leqslant w \leqslant D$ | $0 \leqslant w \leqslant D$ | $x_{on} \leqslant x \leqslant x_{off}$ | $x_{on} \leqslant x \leqslant x_{off}$ | $0 \leqslant x \leqslant 1$ | $0 \leqslant w \leqslant D$ |
| Control mechanism | Current controlled | Voltage controlled | Current controlled | Voltage controlled | Voltage controlled | Voltage controlled |
| I-V relationship | Explicit | Explicit | Explicit | Explicit | Explicit | Explicit |
| Memristance change | Explicit | Explicit | Explicit | Ambiguous | Ambiguous | Explicit |
| Threshold charateristics | No | No | Threshold currents | Threshold voltages | Threshold voltages | Threshold voltages |
| Read/Write circuits | Available | Available | Available | Available | Available | Available |
| Logic circuits | Unavailable | Unavailable | Available | Available | Available | Available |
| Neural synaptic circuits | Unavailable | Unavailable | Unavailable | Unavailable | Unavailable | Available |

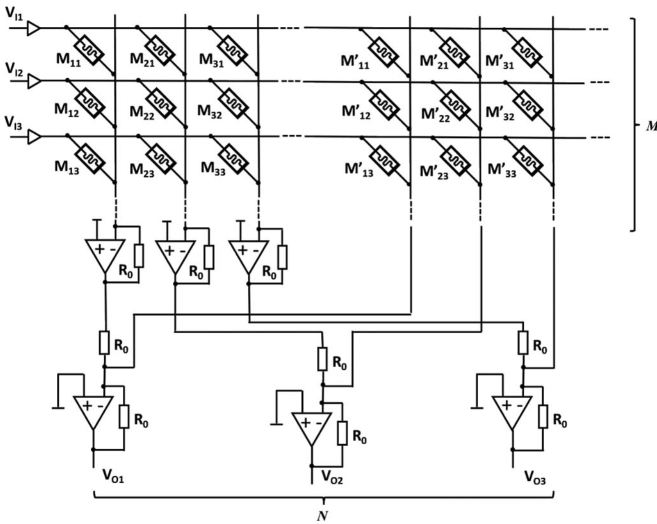


Fig. 6. Proposed synaptic circuits.

The synaptic weight is

$$W_{ji} = R_0 \times \left(G_{ji} - G'_{ji}\right). \quad (9)$$

The proposed synaptic circuit requires fewer amplifiers and resistors, as compared with the work in [5], reducing area and power dissipation.

According to experimental data [shown in Fig. 3(b)], the memristance of an AIST-based memristor can be changed by applying different voltages. When the input voltage is a positive square wave pulse with magnitude of $+0.6$ V and width of 0.25 ms, the memristance of the AIST-based memristor changes from $R_{\mathrm{OFF}}$ to $R_{\mathrm{ON}}$, as shown in Fig. 3. When the input voltage is a negative square wave pulse with magnitude of $-0.6$ V and width of 0.25 ms, the memristance of the AIST-based memristor changes from $R_{\mathrm{ON}}$ to $R_{\mathrm{OFF}}$.

## *B. Weight Change Process*

When the synaptic weight changes, for example, if $\Delta W_{22} > 0$, $M_{22}$ decreases or $M'_{22}$ increases. Similarly, if $\Delta W_{22} < 0$, $M_{22}$ increases or $M'_{22}$ decreases. Consider the weight changes in the positive memristor-based crossbar array $(M^{+}(G_{ji}))$. If $\Delta W_{22} > 0$, weight change voltage $V > 0$. Assume only

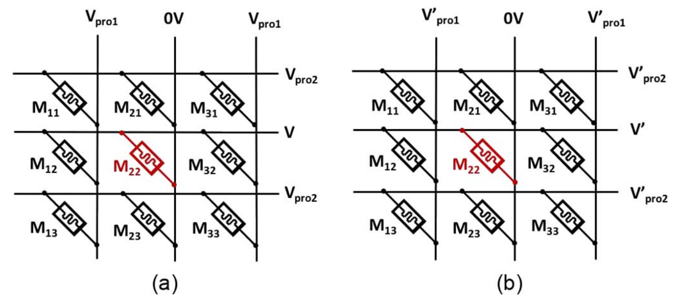


Fig. 7. Proposed weight change in the memristor-based crossbar. (a) Weight increases. (b) Weight decreases.

memristor $M_{22}$ changes and the remaining memristors are unchanged. One possible solution is to apply different voltages on different rows and columns. Weight change voltage $V$ and protect voltages $V_{\mathrm{pro2}}$ are applied to, respectively, row 2 and the other rows. Protect voltages $V_{\mathrm{pro1}}$ and 0 V are applied, respectively, to the other columns and column 2, as shown in Fig. 7(a). The positive and negative threshold voltages of the synaptic memristors are, respectively, $V_{T+}$ and $V_{T-}$. Only the voltage of memristor $M_{22}$ is larger than $V_{T+}$, which is voltage $V$. The memristance of $M_{22}$ therefore decreases. The voltage of memristors, $M_{11}$, $M_{13}$, $M_{31}$, and $M_{33}$, is equal to $V_{\mathrm{pro2}} - V_{\mathrm{pro1}}$, and the absolute value is smaller than $V_{T-}$. The voltage of memristors, $M_{12}$, $M_{32}$, is $V - V_{\mathrm{pro1}}$ and smaller than $V_{T+}$. The voltage of memristors, $M_{21}$ and $M_{23}$, is $V_{\mathrm{pro2}}$ and smaller than $V_{T+}$. The memristances therefore remain unchanged. The constraint conditions are

$$\begin{cases} V > V_{\mathrm{pro1}} > V_{\mathrm{pro2}} \geqslant 0 \\ V_{\mathrm{pro2}} < V_{T+} \\ V_{\mathrm{pro2}} - V_{\mathrm{pro1}} > V_{T-} \\ V - V_{\mathrm{pro1}} < V_{T+} \\ V > V_{T+}. \end{cases} \quad (10)$$

Similarly, if $\Delta W_{22} < 0$, the weight change voltage $V' < 0$. The weight change voltage $V'$ and protect voltages $V'_{\mathrm{pro2}}$ are applied, respectively, to row 2 and the other rows. Protect voltages $V'_{\mathrm{pro1}}$ and 0 V are applied, respectively, to the other columns and column 2, as shown in Fig. 7(b). Only the voltage of memristor $M_{22}$ is smaller than $V_{T-}$. The memristance of $M_{22}$ therefore increases. The voltage of memristors, $M_{11}$, $M_{13}$,

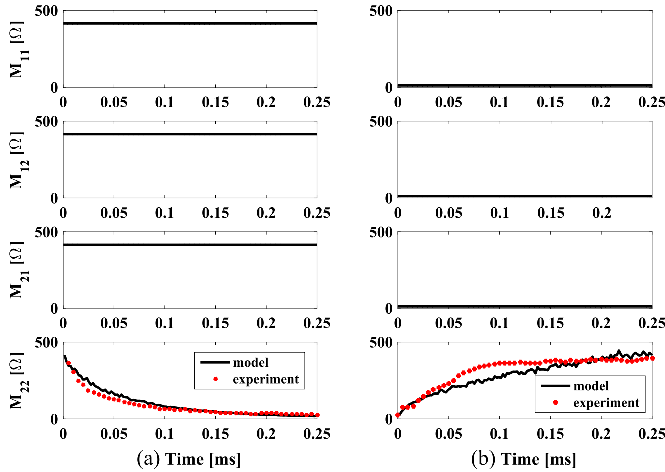


Fig. 8. Change in synaptic weight of memristor $M_{22}$ with 20% memristance variations in the synaptic crossbar array. (a) Increase in weight. (b) Decrease in weight.

$M_{31}$, and $M_{33}$, is $V'_{\text{pro2}} - V'_{\text{pro1}}$ and smaller than $V_{T+}$. The voltage of memristors, $M_{12}$ and $M_{32}$, is $V' - V'_{\text{pro1}}$, and the voltage of memristors, $M_{21}$ and $M_{23}$, is $V'_{\text{pro2}}$. The absolute value of the voltages is smaller than $V_{T-}$. The memristance therefore remains the same. The constraint conditions are

$$\begin{cases} V' < V'_{\text{pro1}} < V'_{\text{pro2}} \leqslant 0 \\ V'_{\text{pro2}} > V_{T-} \\ V'_{\text{pro2}} - V'_{\text{pro1}} < V_{T+} \\ V' - V'_{\text{pro1}} > V_{T-} \\ V' < V_{T-}. \end{cases} \tag{11}$$

## IV. Experimental and Simulation Verification

Electrical characterization is performed using a probe station (Cascade S300) equipped with a semiconductor characterization system (Keithley 4200-SCS) under the pulse voltage sweep mode. During electrical measurements, the positive bias is the current flowing from the Ta electrode to the bottom Ag electrode. All measurements are performed at room temperature in air. PSPICE is used to evaluate the proposed memristor model and crossbar circuits. The parameters of the AIST-based memristor are listed in Table I.

With the aforementioned method for changing the weight, the simulation results demonstrate that only $M_{22}$ can be changed (see Fig. 8) while the other devices remain in the same state during the weight change process. The amplitude of the applied positive input voltage is 0.6 V or −0.6 V, and the width is 0.25 ms according to Fig. 3. To consider practical conditions, 20% memristance variations are included in the model during the weight change process. The change in memristance in the proposed model matches the experimental data within 18% accuracy, as shown in Fig. 8.

Different sizes of crossbar architectures have been verified, and a similar conclusion is noted that the memristance of the unselected memristors does not change during the weight change process.

## V. Conclusion

A memristive model has been presented for memristor-based synaptic circuits. The model is based on experimental data of practical memristive devices and matches the $I-V$ characteristics of both sinusoidal and repetitive sweeping inputs and changes due to voltage pulses. The model can also be tuned to describe memristors composed of different materials. The proposed synaptic circuit requires fewer amplifiers and resistors as compared with [5], reducing area and power dissipation. Moreover, the robustness of the model is verified by 20% additive memristance variations. The accuracy of the model is within 18%, and the proposed synaptic circuits can be used within crossbar arrays of memristive neural networks.


## Acknowledgment

The authors would like to thank the Center for Nanoscale Characterization and Devices of WNLO for the facility support.


## References


[1] K. J. Kuhn, "Considerations for ultimate CMOS scaling," *IEEE Trans. Electron Devices*, vol. 59, no. 7, pp. 1813–1828, Jul. 2012.

[2] L. O. Chua, "Memristor—The missing circuit element," *IEEE Trans. Circuit Theory*, vol. CT-18, no. 5, pp. 507–519, Sep. 1971.

[3] D. B. Strukov, G. S. Snider, D. R. Stewart, and R. S. Williams, "The missing memristor found," *Nature*, vol. 453, no. 7191, pp. 80–83, Mar. 2008.

[4] P. Junsangsri and F. Lombardi, "Design of a hybrid memory cell using memristance and ambipolarity," *IEEE Trans. Nanotechnol.*, vol. 12, no. 1, pp. 71–80, Jan. 2013.

[5] M. Hu, H. Li, Y. Chen, Q. Wu, G. S. Rose, and R. W. Linderman, "Memristor crossbar-based neuromorphic computing system: A case study," *IEEE Trans. Neural Netw. Learn. Syst.*, vol. 25, no. 10, pp. 1864–1878, Oct. 2014.

[6] Z. Biolek, D. Biolek, and V. Biolkova, "SPICE model of memristor with nonlinear dopant drift," *Radioengineering*, vol. 18, no. 2, pp. 210–214, Jun. 2009.

[7] D. Batas and H. Fiedler, "A memristor SPICE implementation and a new approach for magnetic flux-controlled memristor modeling," *IEEE Trans. Nanotechnol.*, vol. 10, no. 2, pp. 250–255, Mar. 2011.

[8] S. Kvatinsky, E. G. Friedman, A. Kolodny, and U. C. Weiser, "TEAM: ThrEshold adaptive memristor model," *IEEE Trans. Circuits Syst. I, Reg. Papers*, vol. 60, no. 1, pp. 211–221, Jan. 2013.

[9] S. Kvatinsky, M. Ramadan, E. Friedman, and A. Kolodny, "VTEAM—A general model for voltage controlled memristors," *IEEE Trans. Circuits Syst. II, Express Briefs*, vol. 62, no. 8, pp. 786–790, Aug. 2015.

[10] C. Yakopcic, T. M. Taha, G. Subramanyam, and R. E. Pino, "Generalized memristive device SPICE model and its application in circuit design," *IEEE Trans. Comput.-Aided Des. Integr. Circuits Syst.*, vol. 32, no. 8, pp. 1201–1214, Aug. 2013.

[11] Y. Li *et al.*, "Ultrafast synaptic events in a chalcogenide memristor," *Sci. Rep.*, vol. 3, p. 1619, Apr. 2013.

[12] Y. Li *et al.*, "Activity-dependent synaptic plasticity of a chalcogenide electronic synapse for neuromorphic systems," *Sci. Rep.*, vol. 4, p. 4906, May 2014.

[13] A. M. Sheri, H. Hwang, M. Jeon, and B.-G. Lee, "Neuromorphic character recognition system with two PCMO memristors as a synapse," *IEEE Trans. Ind. Electron.*, vol. 61, no. 6, pp. 2933–2941, Jun. 2014.

[14] M. Chu, B. Kim, S. Park, H. Hwang, M. Jeon, and B. Lee, "Neuromorphic hardware system for visual pattern recognition with memristor array and CMOS neuron," *IEEE Trans. Ind. Electron.*, vol. 62, no. 4, pp. 2410–2419, Apr. 2015.

[15] S. Choi, P. Sheridan, and W. D. Lu, "Data clustering using memristor networks," *Sci. Rep.*, vol. 5, p. 10 492, May 2015.

[16] S. P. Adhikari, M. P. Sah, H. Kim, and L. O. Chua, "Three fingerprints of memristor," *IEEE Trans. Circuits Syst. I, Reg. Papers*, vol. 60, no. 11, pp. 3008–3021, Nov. 2013.